# An Accelerated Wound-Healing Surgical Suture Engineered with an Extracellular Matrix

*by* Agustina Setiawati

**Submission date:** 31-Jan-2023 07:10PM (UTC+0700)
**Submission ID:** 2003266600
**File name:** Engineered_with_an_Extracellular_Matrix-annotated-annotated.pdf (3.33M)
**Word count:** 9287
**Character count:** 47789

ADVANCED HEALTHCARE MATERIALS
www.advhealthmat.de

# An Accelerated Wound-Healing Surgical Suture Engineered with an Extracellular Matrix

*Agustina Setiawati, Dongyoon Jang, Daeyon Cho, Shingyu Cho, Hayan Jeong, Sungmin Park, Jungsug Gwak, Soo Ryeon Ryu, Won Hee Jung, Bong-Gun Ju, Kwang-Hwan Jung, Oh-Sun Kwon, and Kwanwoo Shin**

**A suture is a ubiquitous medical device to hold wounded tissues together and support the healing process after surgery. Surgical sutures, having incomplete biocompatibility, often cause unwanted infections or serious secondary trauma to soft or fragile tissue. In this research, UV/ozone (UVO) irradiation of polystyrene sulfonate acid (PSS) dip-coating is used to achieve a fibronectin (FN)-coated absorbable suture system, in which the negatively charged moieties produced on the suture cause fibronectin to change from a soluble plasma form into a fibrous form, mimicking the actions of cellular fibronectin upon binding. The fibrous fibronectin coated on the suture can be exploited as an engineered interface to improve cellular migration and adhesion in the region around the wounded tissue while preventing the binding of infectious bacteria, thereby facilitating wound healing. Furthermore, the FN-coated suture is found to be associated with a low friction between the suture and the wounded tissue, thus minimizing the occurrence of secondary wounds during surgery. It is believed that this surface modification can be universally applied to most kinds of sutures currently in use, implying that it may be a novel way to develop a highly effective and safer suture system for clinical applications.**

The suture is a ubiquitous medical device used to close and support wounded tissue during the healing process after surgery.[1] Various absorbable and non-absorbable polymers, natural, or synthetic polymers with mono- or multi-filament structures, are commonly used as suture materials.[2] Because non-absorbable sutures, such as nylon, silk, and polypropylene, have long-term biocompatibility issues and need to be removed in revision surgery, new research directions or technological advances are needed to address these weaknesses.[3] On the other hand, absorbable sutures, such as polydioxanone (PDO), polyglycolic acid (PGA), and polyglactin 910 (PGLA), are still in need of further technological development, despite the advantage that minimal postoperative treatment is required; the decomposition time must be consistent with tissue recovery stages, and their metabolite product should be non-toxic to the human body. To meet clinical requirements, researchers have investigated extensively the biocompatibility,[4] biodegradability and mechanical strength[5] of absorbable sutures.

Recently, studies have been conducted in new directions, and attaching drugs or biological molecules[4] to surgical sutures has been reported to hold promise for developing a delivery platform that will enhance wound healing.[2,6] Despite efforts to implement drug-releasing functions with sutures, fundamental problem remains. During surgery, friction at the interface between the tissue and the suture, which can trigger serious "secondary trauma" to soft or fragile tissue, is always present to some degree[7] and can cause inflammation, pain[8] and infection at the surgery site, resulting in a longer healing time. For instance, lubricating a suture with an antibiotic or with dopamine hydrochloride (DA) and carboxymethyl cellulose (CMC) can reduce the friction coefficient and the tissue drag, as well as improve the ability of the suture to glide through the tissue.[9] Therefore, an ideal modification for the surface of a suture should not only decrease the friction force at the suture–tissue interface to minimize scar formation but also increase biofunctionality and biocompatibility to enhance would healing.

The wound healing of tissue injured during surgery has three dynamic phases, inflammation, proliferation and remodeling, in which fibroblasts are the key players.[10] During late inflammation and proliferation, fibroblasts degrade fibrin clotting by

A. Setiawati, D. Jang, D. Cho, Dr. S. R. Ryu, Dr. O.-S. Kwon, Prof. K. Shin
Department of Chemistry and Institute of Biological Interfaces
Sogang University
35 Baekbeom-ro, Mapo-gu, Seoul 04107, Republic of Korea
E-mail: kwshin@sogang.ac.kr
A. Setiawati, S. Cho, H. Jeong, Dr. J. Gwak, Prof. B.-G. Ju, Prof. K.-H. Jung
Department of Life Science
Sogang University
35-Baekbeom-ro, Mapo-gu, Seoul 04107, Republic of Korea
A. Setiawati
Faculty of Pharmacy
Sanata Dharma University
Paingan, Maguwoharjo, Depok, Sleman, Yogyakarta 55284, Indonesia
S. Park, Prof. W. H. Jung
Department of Systems Biotechnology
Chung-Ang University
Anseong 17546, Republic of Korea
The ORCID identification number(s) for the author(s) of this article can be found under https://doi.org/10.1002/adhm.202001686

DOI: 10.1002/adhm.202001686

releasing matrix metalloproteinase (MMP) and then replacing it with extracellular matrix (ECM) compounds.[10] Once the ECM organization has been fully restored, newly formed tissue will have the same strength and functions as the original tissue. In a previous study, ECM organization was successfully restored by incorporating matrix metalloproteinase inhibitor into the suture's surface and by coating the suture's surface directly with ECM compounds like collagen and laminin.[5,11] Fibronectin (FN), a glycoprotein found in anionic proteoglycan (PG)-rich extracellular regions, is an abundant ECM compound and plays a crucial role in wound healing.[12,13] In late wound healing responses, fibroblast-released globular cellular fibronectin (FN) assembles into a three-dimensional fibrillar structure that plays an important role in regulating the composition of the ECM and the deposition of its components, including collagen types I and III, fibrinogen, fibrillins 1 and 2, fibullin, tenascin-c and laminin.[14] Interestingly, FN is also known to have a lubricating property when combined with synovial fluid components.[15]

As the basis of this study, we hypothesize that the presence of unfolded FN on the surface of a suture can improve biocompatibility and stimulate cellular activity to accelerate wound healing. In a previous study, FN was successfully adsorbed onto the suture's surface by using polystyrene sulfonate (PSS) and UV/ozone (UVO) irradiation; this provided negative charges on the suture and subsequently induced the unfolding of FN by electrostatic interactions to domain $I_{1-5}$ and $III_{10}$ of the FN molecule.[16,17] This method is universally applicable to any type of suture regardless of its structure, size and degradability. We found that a polydioxanone (PDO) suture with adsorbed FN had improved biocompatibility because it attracted fibroblasts while impeding the binding of *Staphylococcus aureus* (*S. aureus*) and *Escherichia coli* (*E. coli*) with the surface of the suture. The healing functionalities of PDO sutures with adsorbed FN were investigated by measuring the fibroblast migration rate in scratch assays in vitro, assessing the degree of skin tissue regeneration, and calculating the Scar Index in a stitched mice model in vivo. Our result revealed better wound healing activity and less scarring for PDO sutures with adsorbed FN than for the control PDO sutures. Thus, we could infer that adsorbed FN had been released to the surrounding area, enabling fibroblast migration, and initiating wound closure. Finally, the use of the suture with surface modification potentially minimized tissue damage by reducing friction between the suture and tissue due to the lubrication effect provided by the modified surface. Our result highlights that surgical sutures with adsorbed FN are a simple, versatile alternative to the usual sutures and that such modified sutures will promote greatly accelerated wound healing.

We modified the surfaces of sutures with either polystyrene sulfonate acid (PSS), an anionic derivative of polystyrene (PS), as a biomimetic analogue to negatively charged sulfonated PGs such as heparin sulfate, or with UV/ozone (UVO) irradiation to produce hydroxy (OH) and carbonyl (C=O) groups as analogues to negatively charged chondroitin sulfate, as described in **Figure 1**a. In the case of PSS dip-coating, we used PSS containing 33 mol% of sulfonate groups, which was found in our previous study to initiate successful FN network formation.[17] PSS facilitated FN adsorption and fibrillogenesis via electrostatic interactions with the excess positive charges in domains $I_{1-5}$ and $III_{10}$ in the FN molecule.[16] On the other hand, ozone absorbs 254-nm UV light to form atomic oxygen that reacts with water molecules to generate hydroxyl radicals that are a strong oxidizing agent.[18] Subsequently, UVO irradiation induces negative charge[19,20] through the introduction of hydroxy and carbonyl groups on the surface of the target polymer.[21] Both methods open cryptic domains of the FN molecule, which are crucial to the binding of $\alpha5\beta1$ and $\alpha v\beta3$ integrin receptors of cells.[16] Because prolonged UVO irradiation causes damage to the surface of polydioxanone (PDO) (Figure S1, Supporting Information), we used an irradiation time of two minutes.

To confirm the successes of the PSS dip-coating and the UVO irradiation in generating negative functional groups on the surfaces of the sutures and subsequently initiating FN adsorption, we used Fourier transform infrared (FTIR) spectroscopy to compare the sutures at each step of the two treatments. The peaks at 680 and 1109 $cm^{-1}$ corresponding to the -CS stretching band and the S-phenyl group, respectively, confirmed the presence of sulfone groups on the surfaces of the sutures that had been dip-coated with PSS while the peak at ≈3600 $cm^{-1}$ corresponding to the −OH stretching band confirmed the presence of oxidation on the surfaces of the UVO-treated sutures. The FTIR results obtained after the treatments pointed to the presence of substantial amounts of incorporated FN, as evidenced by the amide I peaks at 1653 and 1651 $cm^{-1}$ and the amide II peaks at 1547 and 1553 $cm^{-1}$. FN adsorption was further confirmed by the presence of amide A peaks at 3271 $cm^{-1}$ and at 3274 $cm^{-1}$ on the surfaces of the PSS-treated and the UVO-treated sutures, respectively (Figure 1b). We also found that the two processes can be universally applied to various commercial sutures, regardless of their structures, sizes, and degradability in the human body (Figure S2 and Table S1, Supporting Information). The results of quantitative analyses showed that the FN amounts on UVO-irradiated ($34.22 \pm 1.15$ ng $mm^{-2}$) and PSS-coated ($48.28 \pm 0.98$ ng $mm^{-2}$) sutures were significantly higher than the amount on the control suture, the untreated PDO suture ($14.70 \pm 1.12$ ng $mm^{-2}$) ($p < 0.01$) (Figure 1c).

To investigate whether the negative charges on the engineered PDO surfaces could induce protein unfolding of FN upon adsorption, we performed fluorescence resonance energy transfer (FRET) assays and calculated the FRET ratio ($I_A/I_D$). The folded quaternary FN revealed strong energy transfer with an $I_A/I_D$ value of $1.06 \pm 0.05$ while energy transfer was reduced due to extended conformations in 6-M GdnHCl ($I_A/I_D$ $0.27 \pm 0.01$). The UVO-derived charges unfolded the FN confirmation, resulting in an $I_A/I_D$ value of $0.51 \pm 0.04$, whereas the presence of strong negative charges in PSS induced even more significant FN conformational change, resulting in a reduced $I_A/I_D$ value of $0.28 \pm 0.04$ (Figure 1d). SEM images of the UVO- and PSS-treated sutures further confirmed that the unfolded FN molecules formed an extended fibrillar matrix on the modified sutures, which was in good agreement with the previously observed morphologies,[16] while intact, globular FN molecules on the non-charged pristine PDO suture were clustered in island-like aggregates (Figure 1e; Figure S3, Supporting Information). In addition, we confirmed that the FN fibrillar structures occupied a larger area in the engineered sutures; the high-resolution SEM images in Figure 1e showed higher FN coverages of $13.3 \pm 2.2\%$ and $21.1 \pm 3.6\%$ respectively for the UVO- and PSS-treated sutures, but only $6.1 \pm 1.6\%$ for the untreated suture.

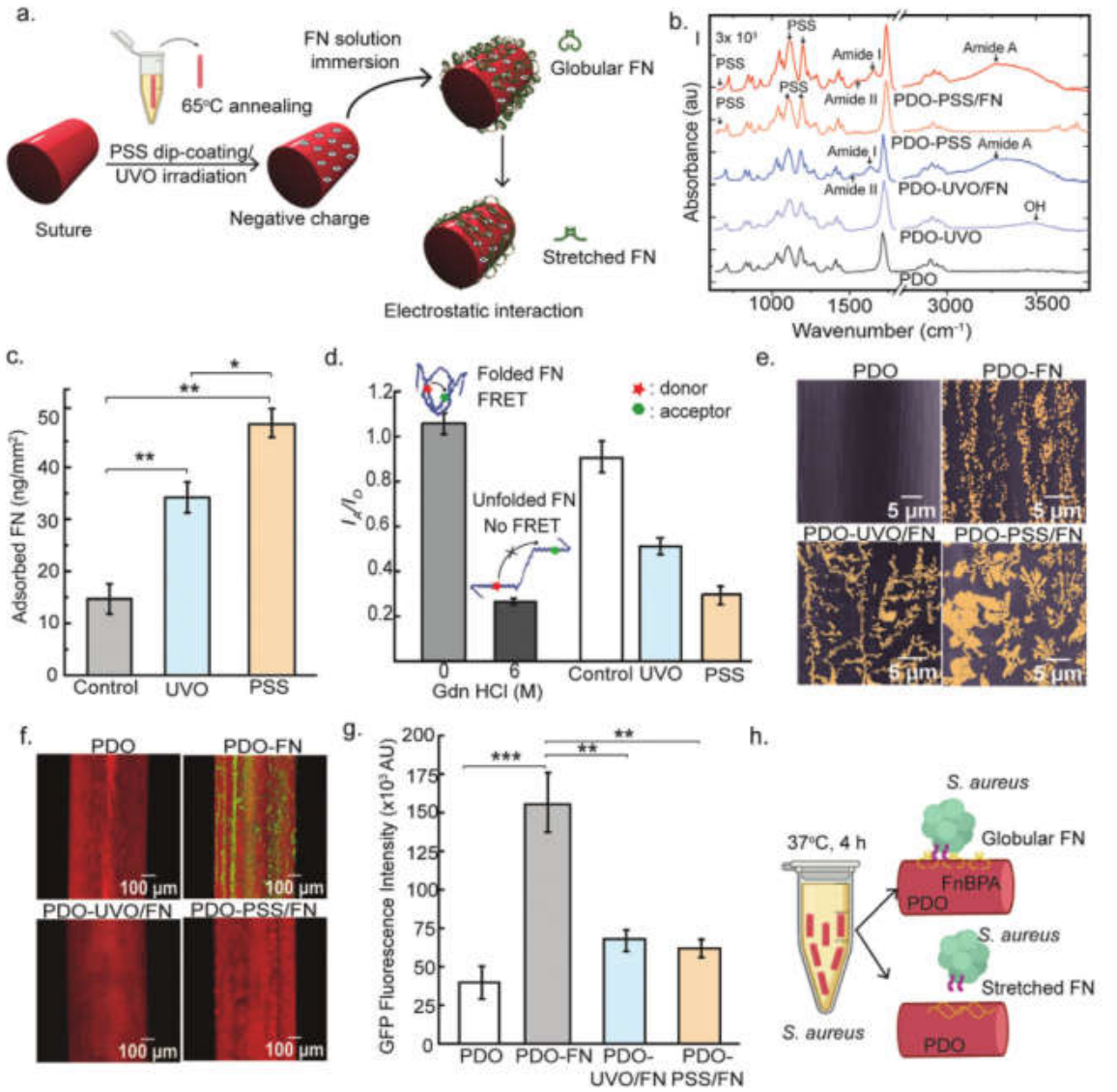


**Figure 1.** Fabrication of a surface-modified suture and confirmation of the presence of unfolded FN on its surface. a) Schematics of the process for fabricating FN-coated sutures. b) FTIR spectra for the surfaces of PDO, PDO-UVO, PDO-UVO/FN, PDO-PSS, and PDO-PSS/FN sutures. Black arrows indicate -CS peaks of PSS; −OH peak from UVO oxidation; amide I, amide II and amide A of fibronectin. c) Amount of FN adsorbed on surface-modified PDO ($n = 4$) Statistical significance was determined using a one-way ANOVA followed by the Tukey test; * $p < 0.05$, ** $p < 0.01$, and *** $p < 0.001$. d) Results of Föster resonance energy transfer (FRET) measurements for the analysis of FN conformation on the surface-modified PDO. Schematics showing the folded and unfolded of FN in donor–acceptor energy transfer on top of the bar charts. e) Representative false colored SEM images of FN (orange) on surface-modified PDO. f) Representative confocal images of *S. aureus* (green) binding on surface-modified PDO (red). g) Quantification of the GFP-expressing *S. aureus* on surface-modified PDO sutures ($n = 3$). Statistical significance was determined using a one-way ANOVA followed by the Tukey Test; * $p < 0.05$, ** $p < 0.01$, and *** $p < 0.001$. h) Schematic of an *S. aureus* binding assay on surface-modified PDO. The illustrations of bacteria were provided by BioRender. c,d,g) Error bars indicate means ± standard deviation (S.D.).

We asked whether the mechanical stretching of the FN molecules on the engineered surfaces of the PDO sutures could disrupt binding to *S. aureus*,[22] which often causes an opportunistic infection and leads to skin abscesses. As shown in Figure 1f (Movies S1 and S2, Supporting Information) and quantified in Figure 1g, the UVO-irradiated and the PSS-coated sutures prevented *S. aureus* binding, as evidenced by decreases in the GFP fluorescence intensity to 66.85 ± 7.02×10$^3$ AU and 61.97 ± 5.92×10$^3$ AU, respectively; furthermore, those surface-modified sutures were more effective than the unmodified control suture (PDO-FN, 155.41 ± 2.66×10$^3$ AU). Of note is that the pristine PDO fiber has the lowest binding of 39.72 ± 10.63×10$^3$ AU. In nature, *S. aureus* binds to FN molecules mediated by fibronectin protein binding A (FnBPA) through a low homophilic bond.[23] However, *S aureus* does not have an affinity to PDO, but rather naturally binds to globular FN rather than stretched FN (Figure 1h). In addition to positive-gram bacteria like *S aureus*, the FN structure reveals binding domains for various negative-gram bacteria for internalization. For instance, *E. coli* binds to FN molecules through adhesive molecules called long polar fimbriae (lpf1) and curli, which mediate internalization to eukaryote cells.[24,25] This study further assessed GFP-expressing *E. coli* binding to the surface-modified PDO sutures (Figure S4, Supporting Information). Interestingly, both the UVO-irradiated and the PSS-coated sutures also exhibited mild binding to *E. coli*, as evidenced by decreases in the average of GFP fluorescence intensity to 11.75.85 ± 2.46×10$^3$ AU and 12.27 ± 2.22×10$^3$ AU, respectively. These values were significantly lower than the values of 137.00± 4.78×10$^3$ AU for the PDO-FN sutures and 89.28 ± 18.78×10$^3$ AU for the PDO control sutures. We confirmed that the presence of negative charges on the engineered surfaces of the sutures induced the stretching of FN molecules and the adsorbed FN fibrillar networks prevented the unwanted binding of infectious bacteria very effectively.

The performance of a suture is commonly evaluated by its biocompatibility, which refers to a good interaction between the biomaterial and the biological cells for a specific biomedical purpose.[26] To meet such requirements, sutures have been primarily evaluated based on interactions between the surface of the suture and biological fluids such as water, saline and serum.[27] We found that PSS dip-coating and UVO irradiation of PDO surfaces significantly increased their hydrophilicity by decreasing the contact angles in water, saline (NaCl 0.9%) and serum compared to the hydrophilicities of the control sutures. Furthermore, no statistically significant differences were observed between the contact angles on water and on saline for the PDO-PSS and the PDO-UVO sutures before and after FN adsorption (Figure S5a,b, Supporting Information). However, the contact angle on serum for the PDO-PSS suture (65.2 ± 0.7) was significantly higher than that for the PDO-PSS/FN suture (50.8 ± 3.0) (Figure S5c, Supporting Information). Moreover, PSS and FN treatments of the PDO sutures increased the hydrophilicity significantly compared to the values for the UVO- and the FN-treated sutures. Therefore, a PSS coating followed by FN treatment is predicted to have a higher biocompatibility than a PSS coating followed by UVO or FN treatment.

To test the biocompatibility, we seeded fibroblasts in a confocal dish coated with Pluronic F-127. The densities of attached fibroblasts after 24 h for the PDO-UVO/FN and the PDO-PSS/FN sutures were 384.1 ± 80.6 and 447.2 ± 77.8 cells per mm$^2$ (**Figure 2**a,b; Movie S3, Supporting Information), respectively, which were significantly higher than the value for the control sutures of 86.9 ± 8.3 cells per mm$^2$ ($p < 0.01$) (Movie S4, Supporting Information). After 72 h, the cell densities for the PDO-UVO/FN and the PDO-PSS/FN sutures had increased to 1680.7 ± 269.7 ($p < 0.01$) and 2258.7 ± 193.6 cells per mm$^2$ ($p < 0.001$) (Figure 2b, Movie S5, Supporting Information), respectively, while that for the control sutures remained at 461.98 ± 96.77 cells per mm$^2$ (Movie S6, Supporting Information). We further quantified fibroblast attachment and growth on the PDO-UVO and the PDO-PSS sutures without any FN treatment. After seeding for 24 h, the cell density for the PSS-coated sutures (113.5 ± 26.5 cells per mm$^2$) was significantly higher than those for the pristine PDO (10.7 ± 4.8 cells per mm$^2$) and the UVO-irradiated (27.1 ± 11.3 cells per mm$^2$) sutures. Over 72 h, these cells grew more significantly on the PSS-coated sutures to 660.2 ± 34.8 cells per mm$^2$ than they had on the PDO and the UVO-irradiated sutures (14.9 ± 6.1 and 54.8 ± 9.6 cells per mm$^2$, respectively) (Figure S6, Supporting Information), yet much slower than they had on either the FN-treated PSS dip-coated sutures or the FN-treated, UVO-irradiated sutures. This result supports the finding of a previous study that PSS grafting attracted fibroblasts and improved the attachment of polymeric ligaments to bone tissue.[28,29] However, the presence of unfolded FN on the surfaces of the tested sutures was clearly found to improve their biocompatibility dramatically. Also, of note is the observations that neither PSS coating nor UVO irradiation (for 2 min) altered any physical strength properties of the sutures (Figure S7, Supporting Information), indicating that this method affects neither the chemical structures on surface nor the native physical characteristics of the PDO sutures tested.

The presence of biologically active fragments of FN is known to augment cell migration.[16] FN molecules promote fibroblast polarization and high directional persistence in fibroblast migration through interactions with both its cell-binding and heparin-binding domains.[30] We assume that the fibroblasts in proximity to the FN-coated PDO may be responsible for the improved motility, which is one of the crucial factors in tissue regeneration and rapid wound repair. Thus, the effects of the surface-modified PDO sutures on cell migration were evaluated by using in vitro wound healing assays (scratch assays),[31] with fibroblasts being the key players in wound healing. Fibroblasts are known to migrate to the site of a wound within 24–48 h postinjury by expressing matrix metalloproteinase to degrade fibrin clotting and replace it with collagen fiber.[32] The scratch assay was modified based on the width of the scratch (Figure 2c). According to the results, wound closure for the PDO-UVO/FN suture was 13.64 ± 0.77% while that for the PDO-PSS/FN suture was 17.83 ± 0.55%, both of which were significantly higher ($p < 0.001$) than the value (3.05 ± 0.25%) for the unmodified (control) suture (Figure 2d,e). We inferred that some molecular release of the attached FN molecules into the physiological buffer may have occurred. As shown in Figure 2f, the accumulative amounts of released FN for the PDO-UVO/FN suture were 12.2 ± 0.9, 12.4 ± 1.6, and 16.5 ± 2.5 pg mm$^{-2}$ at 6, 12, and 24 h, respectively, while those for the PDO-PSS/FN suture were 13.1 ± 1.3, 17.4 ± 1.1, and 22.0 ± 0.8 pg mm$^{-2}$. It is worth revealing that the total amount of FN released for the PDO-UVO/FN and PDO-PSS/FN sutures at

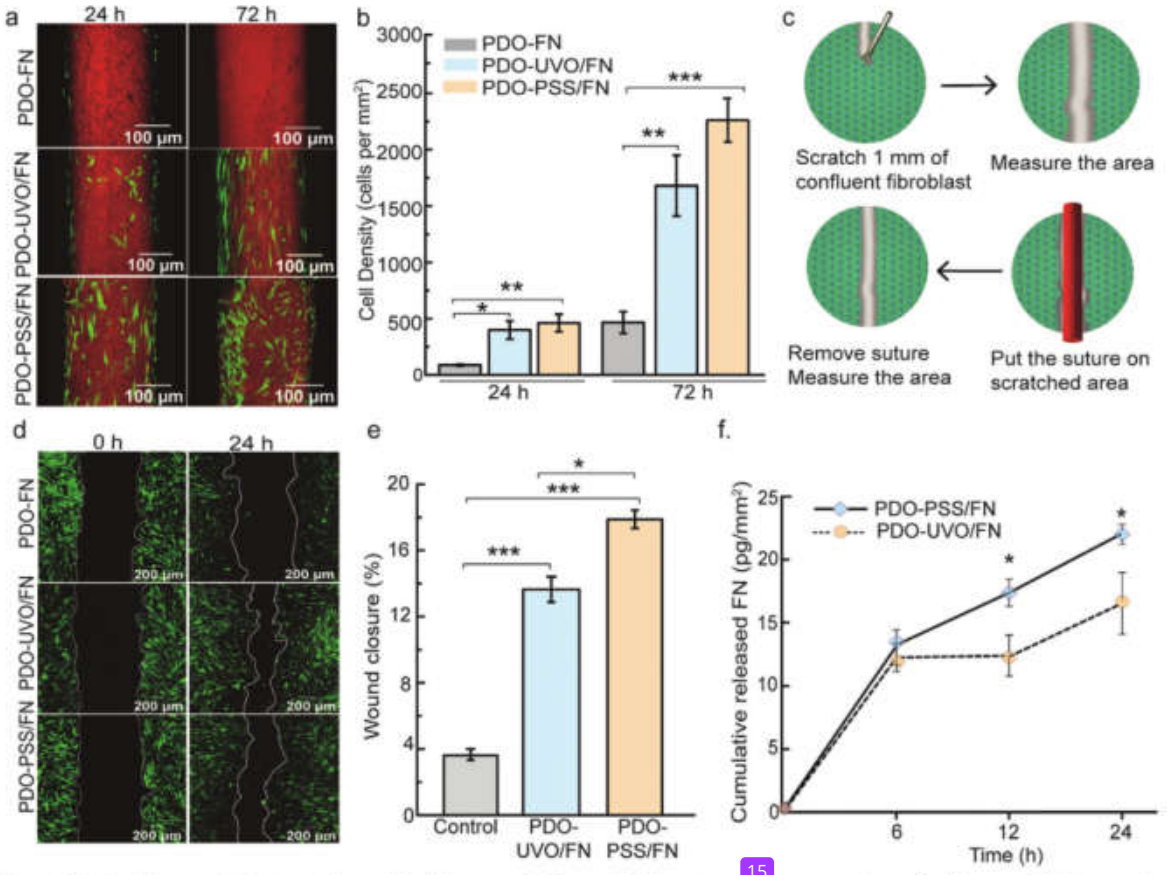


**Figure 2.** In vitro biocompatibility test and wound healing assay of FN-coated PDO sutures. a) Representative confocal images of GFP-expressing fibroblasts (green) grown on PDO-FN, PDO-UVO/FN and PDO-PSS/FN sutures (red) at 24 and 72 h after seeding. b) Fibroblast densities on the suture at 24 and 72 h after seeding. c) Schematics of in vitro wound healing assay. d) Confocal snapshots from in vitro scratch assays, migrating fibroblasts (green) on a culture dish at 0 and 24 h. e) Quantitative analysis of wound closure. f) Cumulative release of fibronectin from modified sutures at 6, 12, and 24 h. Released FN amounts were given by FN mass in pg per suture's surface area in $mm^2$ ($n = 3$). Statistical significance was determined using a one-way ANOVA followed by the Tukey test; $^*p < 0.05$, $^{**}p < 0.01$, and $^{***}p < 0.001$. b,e,f) Error bars indicate means ± S.D.

24 h corresponds to ≈0.53% and 0.46%, respectively of the total amounts of FN preattached to a given suture. The amounts of released FN for the two sutures were meaningfully different at 12 and 24 h ($p < 0.01$). Therefore, we could confirm that the sutures with FN adsorbed were gradually releasing the preattached FN molecules during the wound healing process, thereby improving the migration of the surrounding fibroblasts, and consequently leading to faster wound healing.

Male-BALB/c mice received 4-cm stitches in their dorsal skin by using the surface-modified PDO sutures to assess the in vivo efficacy of those sutures. The wound healing process for these modified sutures was monitored by observing the histology of the wound due to stitching on the dorsal regions of the mice (**Figure 3**a). Before suturing the mice, we used IR spectroscopy to confirm that our modification process had led to the successful adsorption of FN on the surface of the PDO sutures (Figure S8, Supporting Information). After 10 days, the stitched areas were macroscopically and microscopically evaluated. The suture–tissue interface for the surface-modified sutures was observed by cross sectioning the skins of mice taken from the area of the wound.

Macroscopically, the wounded skin showed inflammation as indicated by the black arrows in the images of the dorsal areas (Figure 3b). Inflammation was observed in the areas of mice stitched with the PDO (control) sutures and with the PDO-PSS/FN sutures while very mild inflammation was observed for the mice stitched with PDO-UVO/FN sutures. The process of wound healing was then evaluated using the properties of multiple skin healing parameters; including the epidermis thickness, the formation of granulation tissue, the arrangement of collagen, and scar analyses.[33] As marked in Figure 3c, granulation tissue (GT), composed of tissue matrix (e.g., collagen, fibronectin, and hyaluronic acid) supporting the immune related cells, was found for all suture cases in the region of dermis (D). Notably, more endothelial cells (EC) were found at the mouse skin specimen stitched with the PDO-PSS/FN suture than those with the

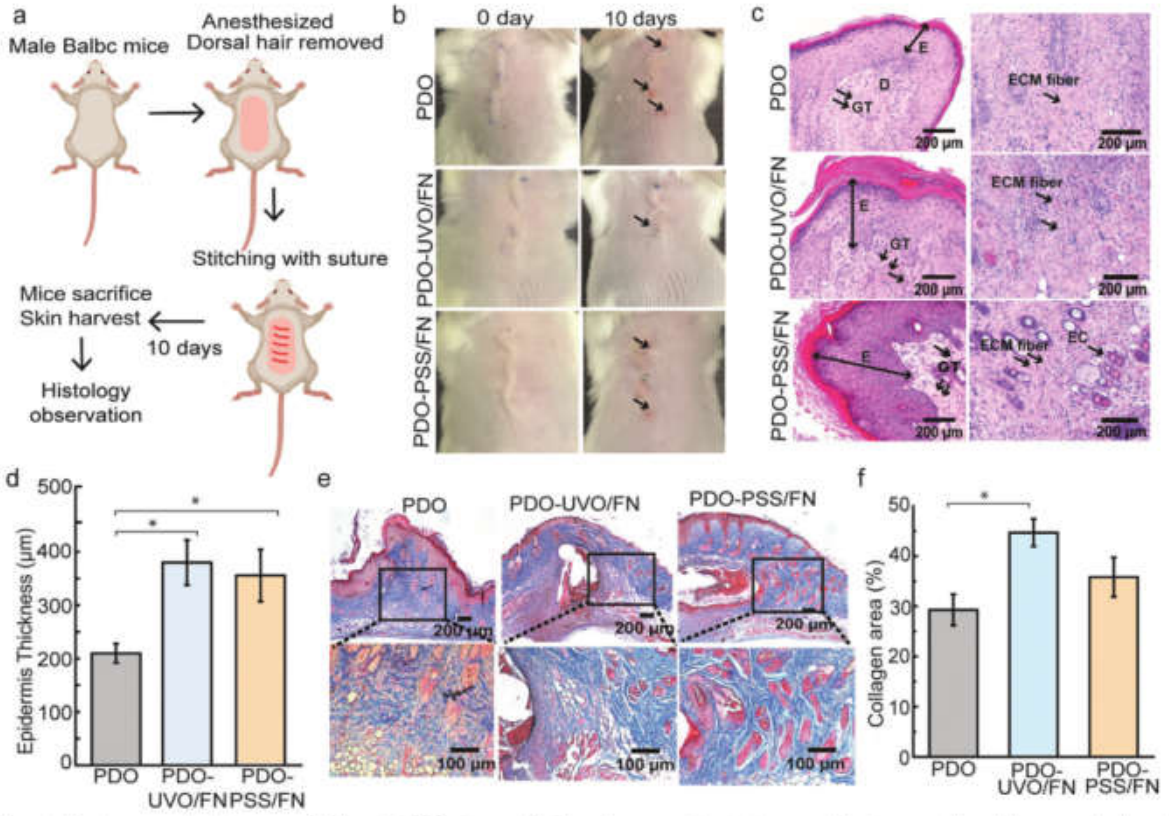


**Figure 3.** In vivo wound healing assays of FN-coated PDO sutures. a) Schematic representing in vivo wound healing assay. The red lines on mice dorsal represent stitched suture. b) Mice skin macroscopy images at days 0 and 10, with the black arrows pointing to the inflammation. c) Histology analysis of H&E-stained cross sections of mouse skin in epidermis (left) and dermis layer (right). E) Black arrows mark epidermis, D) dermis, granulation tissue (GT), endothelial cell (EC) and ECM fiber. Double sided arrow on the left side point out the thickness of epidermis layer. d) Epidermis thickness of the modified sutures, as obtained from mouse-skin histology. e) Representative microscopic images of Masson's trichrome staining of collagen at days 10 postsuturing (up) and corresponding enlarged inserts (bottom). Blue: stained collagen. f) %collagen areas for each type of modified suture ($n = 5$ animals). d,f) Error bars indicate means ± S.D. Statistical significance was calculated using a one-way ANOVA followed by the Tukey test; *$p < 0.05$.

other sutures, which indicated that angiogenesis had occurred more actively (Figure 3c). Meanwhile, epidermis thickness (E) in the histological sections, known as a general indicator for skin healing was evaluated. The newly formed epidermis covers the wound, and consequently protects it from infection.[34] Based on hematoxylin-eosin (H&E) staining, we found epidermis thicknesses of 209.8 ± 18.2, 380.0 ± 42.4, and 355.7 ± 48.8 μm for the PDO, PDO-UVO/FN, and PDO-PSS/FN groups, respectively (Figure 3d). The two surface-treated sutures showed a significantly thicker epidermis than the control suture ($p < 0.05$) as a consequence of re-epithelialization due to cells migrating after injury to the site of the wound.[34]

Specific histology changes, such as flattening of the dermal and epidermal boundaries and the arrangement of collagen bundles, were subsequently observed, and the results from scar analyses were assessed. We found that scar formation for the PDO control suture was noticeably higher than that for any of the modified sutures, as indicated by the flattened tissue areas, marked at dermis-epidermal junction (Figure S9a, Supporting Information). We further evaluated wound scaring by quantifying the Scar Index by dividing the scar area by the corresponding dermis thickness.[35] The PDO-UVO/FN (1152.3 ± 168.0 μm) and the PDO-PSS/FN (960.0 ± 170.3 μm) sutures had lower Scar Indices than the PDO control suture (1544.8 ± 232.9 μm) ($p < 0.05$) (Figure S9b, Supporting Information). Using the degree of collagen deposition and organization, the efficiency of wound healing was further investigated.[36,37] As can be seen in Figure 3e, Masson's Trichrome-stained sections revealed a distinct structural difference in the deposition of collagen fibrils; collagen was abundant, and showed greater in color-depth in specimens stitched with the PDO-UVO/FN and PDO-PSS/FN sutures; and collagen was aligned in ordered configuration, whereas specimen with the PDO control suture was presented as sparse and unorganized collagen bundles. Figure 3f showed % collagen in tissue section; for the PDO-UVO/FN and PDO-PSS/FN sutures, % collagen areas were 44.7 ± 2.8% and 35.8 ± 3.5% respectively, statistically higher than the value of 29.3 ± 3.1% for the control PDO ($P<0.05$). Lastly, a series of inflammation markers,

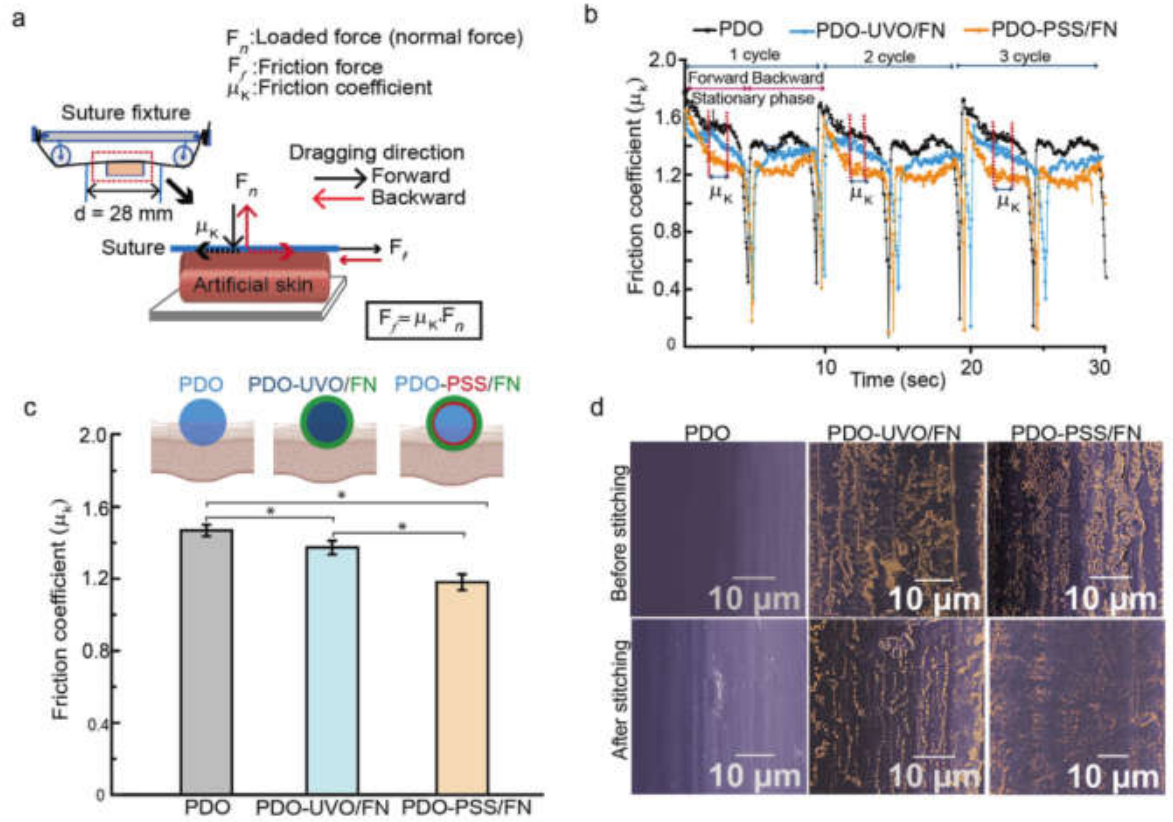


**Figure 4.** Friction test of FN-coated PDO sutures. a) Schematic representing the friction experiment. b) Repeated traces of the friction coefficients as a function of suture–displacement in time (3 cycles). c) Friction coefficients of PDO sutures and of FN-coated PDO sutures (PDO-UVO/FN and PDO-PSS/FN) on Dragon skin 10. Error bars indicate means ± S.D. for $n = 3$ cycles. Statistical significance was calculated using a one-way ANOVA followed by the Tukey test; * $p < 0.05$. Schemes on the top of bar chart representing suture–tissue interface. d) Representative false-colored SEM images of FN molecule (orange) on the surface-modified PDO sutures before and after stitching in mouse skin.

including interleukin-1 (IL-1), interleukin-6 (IL-6), tumor necrosis factor alpha (TNF-α), and vascular endothelial growth factor (VEGF), were evaluated, in order to compare the differences in healing effects.[38,39] The IL-1 level, however, was not measurable due to the very low expression level in all samples, and all other protein levels were not statistically significant between groups (Figure S10, Supporting Information). This may be due to a low inflammatory response to the wound from the suture on the 10th day after suturing. Nevertheless, in line with in vitro study, the results of in vivo wound healing assays supported our hypothesis that the engineered sutures with FN would improve wound healing during postsurgery recovery.

As previously mentioned, friction occurs at the interface between the sutures and the tissues and can cause secondary tissue trauma and infection.[7] During stitching, we notably found that the surface-modified sutures easily glided through mouse skin. In order to confirm this quantitatively, we designed a friction test for artificial skin. Dragon skin 10 was chosen for the artificial skin material, and the carefully measured friction coefficients of the FN-coated sutures were compared, for a normal loading force ($F_n$) and a frictional force ($F_f$), to those of the sutures without FN adsorption (**Figure 4**a; Figure S11, Supporting Information). Once the suture was dragged along tissue's surface, a stick-slip plot was generated, and the result is shown in Figure 4b. The optimal normal load in this study was found to be 0.400 N, and the optimal speed was found to be 3 mm $s^{-1}$. The kinetic friction coefficients ($\mu_K$) for the PDO-UVO/FN and the PDO-PSS/FN sutures were 1.33 ± 0.03 and 1.17 ± 0.04, respectively, which were lower than that of the PDO (control) suture (1.46 ± 0.03) (Figure 4c). The sticky characteristic of silicone rubber caused the $\mu_K$ value (>1.00) to be higher than in previous studies (≈0.100) that used other types of artificial skin. Our FN-coated sutures reduced the friction coefficients from about 0.1–0.30, similar to the reduction in friction coefficients from 0.12 to 0.37 in previously reported study.[7] This confirms that the FN layer on the PDO sutures significantly reduces the friction at the interface with the skin, as previously noticed by the tactile sensations during stitching. Friction at the suture–silicone rubber interface disturbed the coated FN and caused deformation of the PDO (Figure S9b, Supporting Information). SEM images of the surfaces of the sutures after in vivo stitching in mice indicated trends similar to those in the friction test; i.e., some coated FN had peeled off from the

suture's surface (Figure 4d). However, we assume that the FN remaining on the sutures was responsible for the healing of the stitched wounds on the skins of mice. We confirmed that coating with FN provided not only a therapeutic advantage but also a lubrication effect, thereby minimizing tissue defects by behaving like a liquid and lowering the friction force.[40]

In this report, the adsorption of fibronectin by a surgical suture was achieved by using UVO irradiation or a PSS dip-coating. Unfolded and stretched FN molecules on the surfaces of the charged sutures disturb the FN binding domains for *S. aureus* and *E. coli*, preventing the risk of secondary infection during or after the stitching process. These FN molecules also improved the biocompatibility of the sutures by attracting fibroblasts to the wound site. Furthermore, in vitro and in vivo studies of wound healing revealed that the FN-coated sutures enhanced the wound healing process via accelerated re-epithelialization, which may minimize scar formation. Additionally, the FN-coated suture was found to lower the friction at the suture–tissue interface. Most importantly, this approach can be further expanded by incorporating other therapeutic proteins or small molecules to functionalize sutures to improve tissue integration and healing.

## Experimental Section

*Chemicals*: The polydioxanone sutures used in this study (Monosorb, Code DMMV102) were provided by Samyang Biopharmaceuticals. Other various suture materials, polydioxanone (PDS II, W9234), polyglactin 910 (Vicryl, W9440), silk (Mersilk, W605) and polypropylene (Prolene, 8832H), were purchased from Ethicon while silk (Black Silk, SK521), nylon (Blue Nylon, NB428), polyglycolic acid (Surgifit, AV122), and cat gut (Chromic, C5 17) were obtained from Ailee. All suture sizes were based on those listed in The United States Pharmacopeia. The polymer material used for the coating was poly (styrene-*co*-4-styrene sulfonic acid) (PSS33, 33.0 mole% $SO_3H$, Polymer Source P6114-SSO3H) in dimethylformamide (DMF, Sigma D455). Fibronectin was obtained from human plasma (Invitrogen, 33016015). The phosphate buffer saline (PBS) (10010-023) used in this research and the cell culture were purchased from Gibco. Cells for biocompatibility and wound healing assays were GFP-human dermal fibroblast neonatal (Angio-proteomie) maintained in Dubelcco's Minimum Essential Media (DMEM, Gibco) containing 10% fetal bovine serum (FBS, Gibco 16000044) and 1% penicillin-streptomycin-glutamine 100× (Gibco, 10378016). Luria-Bertani (LB), Tryptic Soy Broth (TSB, 22092) and zinc chloride ($ZnCl_2$, 208086) for bacteria media were purchased from Sigma. Cells were cultured in a dish from Corning. Pluronic-127 (P2443), bovine serum albumin (BSA) (A9647), anti-human fibronectin antibody isolated from rabbits (F3648), substrate tetramethylbenzidine (TMB) (T8665), Tween (P1754), paraformaldehyde (P6148), and 2, 2, 2-tribromoethanol (Avertin) (T48402) were purchased from Sigma-Aldrich. The Pierce modified Lowry (P1856006) method was obtained from Thermo Fischer Scientific, and horseradish peroxidase conjugated goat anti-rabbit IgG-HRP (ab6721) was purchased from Abcam. Alexa NHS 488 succinimidyl ester (A20000) and Alexa C5 maleimide 546 (A10258) were supplied by Invitrogen. Silicon rubber for the friction test was provided by Dragon Skin 10.

*Surface Modification of the Suture and Characterization*: The sutures were cut into 2-cm pieces, placed in vacuum-sealed plastic, and kept at −20 °C until they were used. PDO sutures were dip-coated in 33% poly (styrene-*co*-4-styrene sulfonic acid) (PSS33) and then dried overnight in an oven at 65 °C. For another group, sutures were exposed to UV/ozone (UVO cleaner Ahtech AH1700) for 2 min while the PDO sutures for the remaining groups were used without any treatment. All of those pretreated sutures were incubated in 50 μg mL$^{-1}$ of fibronectin in PBS for 72 h at 37 °C under gentle shaking to distribute FN equally over the sutures. After incubation, the sutures were washed in PBS three times for FTIR spectroscopy, the PDO sutures was dried in air, after which attenuated total-reflectance Fourier-transform infrared (ATR-FTIR) spectroscopy measurements were performed using the Agilent Cary 6 10 system in the Advanced Bio-Core Facility at Sogang University; 64 scans in the wavenumber range from 600 to 4000 cm$^{-1}$ were accumulated. The signal range for FN adsorption was confirmed by using the same system to record spectra for the FN solutions.

*Adsorbed Fibronectin Quantification*: The amount of adsorbed FN was quantified based on the Pierce modified Lowry method. Five pieces of 2-cm sutures were incubated in 50 μg mL$^{-1}$ of FN solution at 37 °C. The FN solutions before and after incubation (40 μL) were collected in 96-well plates (SPLs), with three replications for each group. The known concentration of the FN solution was used as the standard in this procedure. Modified Lowry reagent, as much as 200 μL, was added into a well and was gently mixed into the solution by using a mini rocker (Bio-Rad) at room temperature (RT) for 10 min. PBS solution was used as a blank for subtracting the absorbance of every sample. Then, Folin-Ciocalteu reagent was mixed into each well and immediately shaken for 30 seconds. The 96-well plate was covered by aluminum foil to protect it from light and incubated at RT for 30 min. A multi-plate reader (EnSpire, PerkinElmer) was used to measure the absorbance at a wavelength of 750 nm. The standard curve was calculated using the corrected absorbance of the known FN solution. The number of adsorbed FN in μg was determined by subtracting the initial number of the FN solution from the number of the FN solution remaining on the plate. The unit of the adsorbed FN was then converted into ng mm$^{-2}$ by dividing by the suture's surface area.

*Fluorescence Resonance Energy Transfer (FRET) Analysis*: Fibronectin was labeled according the procedure reported by Smith et al. (2007) with Alexa NHS 488 and Alexa C5 maleimide 546.[41] To open the FN structure, up to 8-M guanidine hydrochloride (Gdn HCl) was added in $NaHCO_3$ buffer at pH 8.5. Fibronectin was further labeled with acceptor Alexa C5 maleimide, as much as 30 times the FN molar ratio, for an hour at RT. Excess dye was removed by using dialysis against $NaHCO_3$ buffer three times at two-hour intervals and overnight at 4°C. Moreover, the FN was labeled with 70-fold excess donor Alexa NHS 488, a process that took 2 h. Free dye was removed from the FN-DA by using a PD-10 column that had been equilibrated with PBS. The quantitative ratio of acceptors to donors for each FN dimer molecule was calculated using the absorbance at 280, 495 and 556 nm and the FN molar extinction coefficients. Fibronectin double labeled with 10% glycerol was kept at −20°C until it was used. The acceptor-to-donor fluorescence intensity ratios were measured spectrofluorometrically (Hitachi 7000) by using 0- to 6-M Gdn HCl. The PDO sutures and the modified sutures were incubated under the previously mentioned conditions with 90% unlabeled FN and 10% double-labeled FN. The intensity ratio, $I_A/I_D$, demonstrated the existence of a secondary structure in Gdn HCl. To investigate FN conformation on suture, PDO sutures obtained from Ethicon (PDS II 2-0) were used.

*Modified Suture and Bacteria Interaction*: The plasmid pCM29,[42] which is a *S. aureus–E. coli* shuttle vector for expression of sGFP, was provided by Dr. Alexander Horswill (University of Colorado Anschutz School of Medicine). The pCM29 was transformed into *E. coli* C2925 (dam$^-$/dcm$^-$ *E. coli* K12 derivative; New England Biolabs), and plasmid DNA was purified from the positive transformants by using HiGene Plasmid Mini Prep Kits (BioFact, Daejeon, South Korea) according to manufacturer's instructions. The plasmid purified from *E. coli* C2 was introduced via electroporation into *S. aureus* NCTC8325-4.[43] *E. coli* and *S. aureus* cultured in Luria Bertani (LB) and Tryptic Soy Broth (TSB) supplementing with ampicillin (100 μg mL$^{-1}$) and chloramphenicol (10 μg mL$^{-1}$) at 37°C under shaking whereas enhanced GFP expressing *E. coli* was constructed by first introducing GFP to pET28a at the NdeI and the NotI restriction enzyme sites. Both pKA001[44] and introduced pET28a-EGFP were cut at the XbaI and the NotI restriction enzyme sites. Subsequently, the product containing the histidine tag, the thrombin cleavage site, and the EGFP cloned for the pKA001 vector. The final vector, named pKA28-EGFP, was then transformed to *E. coli* UT5600. A single colony of *E. coli* UT5600 containing pKA28-EGFP was inoculated into Luria Bertani (LB) medium with 50 μg mL$^{-1}$ of ampicillin at 37°C and was spun at 200 rpm for 16 h.

The grown cells were transferred to LB in a 1:100 starter : medium ratio and incubated until $OD_{600}$ reached 0.4 at 37°C at 200 rpm. At that time, 1-mM isopropyl β-D-1-thiogalactopyranoside (IPTG) was added until log phase had been reached. In the late log phase, surface-modified sutures were added into the media and then incubated at 30 °C for 2 h in *S. aureus* or 8 h in *E. coli*. Sutures were washed with Tris-buffered saline (TBS) buffer supplemented with 1-mM $ZnCl_2$ to detach unbound *S. aureus* and *E. coli*. Bound bacteria cells were further observed under a confocal microscope.

*Suture Biocompatibility*: The cells were cultivated in a 100-mm culture dish at 37 °C in 5% $CO_2$ until they had reached 80–90% confluence. The cells were washed using PBS and were detached enzymatically using trypsin-EDTA (0.25%) in DMEM for 3 min. Then, the cells were collected by using centrifugation at 1500 rpm for 3 min (Eppendorf 5810R). The cells ($5\times10^5$) were seeded on a 2-cm suture in a sterile 35-mm confocal dish (SPL, 200350) that had been previously coated with Pluronic-127 5% in distilled water for 30 min. This step was used to ensure that the cells had attached equally over the entire surface of the suture. The prepared sutures were divided into six groups: the PDO, PDO-UVO, PDO-PSS, PDO-FN, PDO-UVO/FN, and PDO-PSS/FN groups. After 12 h, the cell-coated sutures were transferred into a new confocal dish filled with 2 mL of fresh media. Z-stack images of the sutures in each group were subsequently taken using confocal microscopy. The number of cells in the 3D-image of a suture was determined using a 3D object counter plug-in in Image J (Fiji) and properly adjusting the threshold for each stack. For contact angle and tensile strength measurements, PDO sutures (Monosorb) were prepared as previously mentioned. The contact angle was measured using an SEO Phoenix 300 Touch Contact Angle, Image XP 5.6U while the tensile strength was determined using an Optech forcemeter DS2-50N.

*In Vitro Wound Healing Assay*: Wound healing assays were performed by using scratch assays on a cell monolayer that had been modified to quantify the cell migration capability after being exposed to the suture. Briefly, fibroblasts, $1\times10^5$ cells $mL^{-1}$, were seeded in a 35-mm culture dish. After the cells had reached confluence in 10% FBS containing DMEM, they were scratched by using a cell scrapper to create an ~1-mm wound. The cells were gently washed with PBS three times to remove cell debris, and the medium was replaced with one containing 0.5% FBS. The migrating cells were evaluated by measuring the residual gap on five different scratched areas at 0 and 24 h.

*Quantification of Fibronectin Release*: Five pieces of 2-cm sutures were surface-modified and the number of adsorbed FN was calculated as previously mentioned. The fibronectin-coated PDO samples from the no treatment, UVO-treated and PSS pretreatment groups were incubated in PBS solution (pH 7.4, Gibco 10010001) at 37 °C under gentle shaking with a mini rocker (BioRad 1660720). Samples of the solution were collected at 6 h, 12 h and 24 h then kept at 4 °C until the sampling process had been completed. Fibronectin released from the PDO suture was quantitatively determined using competitive enzyme-linked immunosorbent assays (ELISAs) that had been developed initially by Rennard and colleagues.[45] Principally, FN was coated on the bottom of micro-well plate and antibody-sample mixture was incubated on the FN coated micro-well plate. Free antibody bound to bottom FN, while FN binding antibody was removed by washing steps. Secondary antibody-conjugated enzyme and subtrate was further added to form visible complex reaction. The more FN released from modified-suture, the less free antibody to react with TMB substrate to form color reaction. Briefly, a micro titer well plate (SPL) was precoated with FN solution at a concentration 1 μg $mL^{-1}$ in a coating buffer that contained 0.1% bovine serum albumin. The coating process was carried out at 4 °C overnight; the excess fibronectin was washed away three times in Tris-buffered saline and Tween 20 (TBST). The coated plate was blocked with 1% BSA in TBS solution for an hour at RT. After the blocking had been completed, the plate was washed with TBST three times to remove unbound BSA. Then, various concentration of standard solution and sample were prepared by adding 50 μL of the standard solution or 50 μL of the sample solution to 50 μL of anti-fibronectin antibody isolated from rabbits (1:30 000). This mixture was incubated for an hour at RT. After an hour, 100 μL of this mixture was added to each well, and the wells were incubated for an hour at RT. After each well had been washed three times with TBST, horseradish peroxidase conjugated mouse anti-rabbit IgG-HRP was added to each cell, followed by the addition of a tetramethylbenzidine (TMB) substrate and incubation for 30 min. The complex reaction products were dissolved in 1-M HCl, and the absorbance was measured using a multi-plate reader (EnSpire, Perkin Elmer) at 450 nm. The number of released FN was calculated by subtracting remaining FN in the solution from the number of adsorbed fibronectin. The unit of the adsorbed FN was then converted into pg $mm^{-2}$ by dividing by the suture's surface area.

*Suture–Tissue Interface on Stitched Mice*: Animal model experiments were performed using the IACUC protocol (No. IACUC2020_02) approved by Sogang University and in accordance with The Guide for the Care and Use of Laboratory Animals of the National Institutes of Health. Male BALB/c mice 8- to 10-weeks old were adapted in a 12-hour light/dark cycle. The mice were individually caged for at least 24 h before the experiment. The mice were anesthetized using 250 mg $kg^{-1}$ of 2,2,2-tribromoethanol (Avertin) intraperitoneally. Hair on the dorsal part was shaved, and the area was cleaned with povidone iodine. The dorsal parts of the test mice were stitched using PDO-UVO/FN and PDO-PSS/FN sutures, and the dorsal parts of the control mice were stitched using PDO sutures; all PDO sutures used in this research were obtained from Ethicon (PDS II 5-0, W9863T) and were prepared in the same way as previously described. The presence of adsorbed FN on the sutures was confirmed using 458 IR spectra prior to the animal experiment. The mice were resuscitated and monitored daily. After 10 days, 5 mice were sacrificed, and regrown hair was removed. The wounds were excised, along with an area of normal skin ca. 5 mm around the wound, after which the excised tissues were pinned flat on dental wax. Tissues were then fixed in 4% aqueous paraformaldehyde and embedded in paraffin. The cut paraffin sections were stained with hematoxylin-eosin (H&E) and Masson's Trichrome dye. Re-epithelialization was assessed using Image J to analyze the newly formed epithelial layer while the scarring of tissue was evaluated using the Scar Index, which is defined as the scar area ($\mu m^2$) divided by the average dermal thickness (μm) according to previous study.[35] The collagen area was calculated by evaluating blue staining of Masson's Trichrome dye using the color deconvolution Image J in pixels. Collagen area was measured as % collagen area divided by total area of section in 100%.[36]

*Quantitative PCR*: Total RNA was extracted from cells or mouse skin by using Tri-RNA Reagent (Favorgen). First-strand cDNA synthesis from the total 500 ng of RNA was performed with PrimeScript RT master mix (RR036A, Takara). The thermocycling condition was 15 min at 37°C and 5 s at 85°C. A Stratagene Mx3000p qPCR machine (Agilent Technologies) was used to subject the synthesized cDNA to real-time PCR with qPCR 2× Premix SYBR (Enzynomics). The PCR conditions used to amplify all genes were 10 min at 95 °C, 40 cycles at 95 °C for 15 s, and 40 cycles at 64 °C for 40 s. Expression data were calculated from the cycle threshold (Ct) value by using the ΔCt method of quantification. The 18s rRNA was used for normalization. The oligonucleotides are listed in Table S2 in the Supporting Information.

*Friction Behavior between the Suture and the Tissue*: Friction tests were performed using a typical tribological setup.[37] The experimental sample was silicone rubber (Dragon skin 10), which has a biomechanical behavior similar to that of human tissue.[46,47] Dragon skin 10 was prepared using equal weights of parts A and B solution to be mixed for 4 min, followed by degassing for 5 min. The mixture was cured in a polyethylene terephthalate (PET) dish at room temperature and then cut into 20×20×5 $mm^3$ pieces for friction sample measurement. To set up the friction experiment, the surface-modified sutures were cut into pieces of 30 cm in length and placed the pieces in a suture holder. The suture holder was fixed after the suture had come into direct contact with sample's interface. The normal force and the friction force were recorded using a force meter (Optech-Imada DS2-5N) while the vertical dragging movement was driven using a Handpi Mo-HTH unit. The PDO control was loaded with a normal force of 0.1–0.5 N at varying dragging speeds (1–3 mm $s^{-1}$) to determine optimum force and the optimum dragging speed for the experiment. A normal force of 0.4 N and a dragging speed of 3 mm $s^{-1}$ were found to be optimal

conditions for the friction experiments. The kinetic friction coefficient ($\mu_K$) of the surface-modified PDO was calculated using the following equation

$$\mu_K = \frac{\text{Friction force } (F_f)}{\text{Normal force } (F_n)} \quad (1)$$

*Statistical Analysis:* All data in this report presented as means ± standard deviations of the mean (S) based on at least three independent measurements. Obtained data were preprocessed to evaluate outliners. Data were statistically analyzed using the one-way ANOVA followed by the Tukey test, and significance was achieved at $^*p < 0.05$ using Origin 9.0.

## Supporting Information

Supporting Information is available from the Wiley Online Library or from the author.

## Acknowledgements

This work was supported by the Basic Research Program (2018R1A6A1A03024940) of the Ministry of Education and by the Mid-Career Researcher Program (2019R1A2C2084638) of the Ministry of Science and ICT, Korea. A.S received scholarship from the Korean Ministry of Education through the Korean Government's Scholarship Program for Doctoral Degree (KGSP-GRA-2016-263). The authors also thank Samyang Biopharmaceuticals Co. for providing the PDO sutures at no cost and for valuable discussions.

## Conflict of Interest

The authors declare no conflict of interest.

## Data Availability Statement

Research data are not shared.

## Keywords

extracellular matrix (ECM), fibronectin, suture, tissue engineering

Received: September 22, 2020
Revised: January 2, 2021
Published online:

[1] C. K. S. Pillai, C. P. Sharma, *J. Biomater. Appl.* **2010**, *25*, 291.
[2] B. Joseph, A. George, S. Gopi, N. Kalarikkal, S. Thomas, *Int. J. Pharm.* **2017**, *524*, 454.
[3] L. S. Nair, C. T. Laurencin, *Prog. Polym. Sci.* **2007**, *32*, 762.
[4] C. Ai, D. Sheng, J. Chen, J. Cai, S. Wang, J. Jiang, S. Chen, *Int. J. Nanomed.* **2017**, *12*, 7737.
[5] B. Pasternak, A. Missios, A. Askendal, P. Tengvall, P. Aspenberg, *Acta Orthop.* **2007**, *78*, 680.
[6] J. S. Lee, Y. Lu, G. S. Baer, M. D. Markel, W. L. Murphy, *J. Mater. Chem.* **2010**, *20*, 8894.
[7] L. Zhang, W. Li, C. Lin, Z. Zhou, *Tribol. Lett.* **2017**, *65*, 1.
[8] A. L. Tajirian, D. J. Goldberg, *J. Cosmet. Laser Ther.* **2010**, *12*, 296.
[9] S. Viju, G. Thilagavathi, *J. Ind. Text.* **2013**, *42*, 256.
[10] R. T. Kendall, C. A. Feghali-Bostwick, *Front. Pharmacol.* **2014**, *5*, 123.
[11] R. S. Camenzind, T. O. Tondelli, T. Götschi, C. Holenstein, J. G. Snedeker, *Clin. Orthop. Relat. Res.* **2018**, *476*, 1104.
[12] K. E. Kadler, A. Hill, E. G. Canty-Laird, *Curr. Opin. Cell Biol.* **2008**, *20*, 495.
[13] E. A. Lenselink, *Int. Wound J.* **2015**, *12*, 313.
[14] W. S. To, K. S. Midwood, *Fibrog. Tissue Repair.* **2011**, *4*, 21.
[15] R. C. Andresen Eguiluz, S. G. Cook, M. Tan, C. N. Brown, N. J. Pacifici, M. S. Samak, L. J. Bonassar, D. Putnam, D. Gourdon, *Front. Bioeng. Biotechnol.* **2017**, *5*, 1.
[16] N. Pernodet, M. Rafailovich, J. Sokolov, D. Xu, N. L. Yang, K. McLeod, [illegible] *Mater. Res., Part A* **2003**, *64*, 684.
[17] [illegible] L. F. Deravi, S. J. Park, B. E. Dabiri, J. S. Kim, K. K. Parker, K. [illegible] *dv. Mater.* **2015**, *27*, 2838.
[18] [illegible] omero-Sánchez, M. M. Pastor-Blas, J. M. Martín-Martínez, M. J. Walzak, *Int. J. Adhes. Adhes.* **2005**, *25*, 358.
[19] N. Hori, T. Ueno, H. Minamikawa, F. Iwasa, F. Yoshino, K. Kimoto, M. C. Il Lee, T. Ogawa, *Acta Biomater.* **2010**, *6*, 4175.
[20] Y. Wang, J. H. Kim, K. H. Choo, Y. S. Lee, C. H. Lee, *J. Membr. Sci.* **2000**, *169*, 269.
[21] Y. Sakurai, N. Kawashima, Y. Tokuoka, *Colloid Polym. Sci.* **2017**, *295*, 413.
[22] M. Chabria, S. Hertig, M. L. Smith, V. Vogel, *Nat. Commun.* **2010**, *1*, 135.
[23] P. Herman-Bausier, S. El-Kirat-Chatel, T. J. Foster, J. A. Geoghegan, Y. F. Dufrêne, *mBio* **2015**, *6*, 1.
[24] Y. J. Oh, M. Hubauer-Brenner, H. J. Gruber, Y. Cui, L. Traxler, C. Siligan, S. Park, P. Hinterdorfer, *Sci. Rep.* **2016**, *6*, 33909.
[25] U. Gophna, M. Barlev, R. Seijffers, T. A. Oelschlager, J. Hacker, E. Z. Ron, *Infect. Immun.* **2001**, *69*, 2659.
[26] K. L. Menzies, L. Jones, *Optom. Vis. Sci.* **2010**, *87*, 387.
[27] E. M. Hamett, J. Alderman, T. Wood, *Colloids Surf., B* **2007**, *55*, 90.
[28] C. Vaquette, V. Viateau, S. Guérard, F. Anagnostou, M. Manassero, D. G. Castner, V. Migonney, *Biomaterials* **2013**, *34*, 7048.
[29] G. Pavon-Djavid, L. J. Gamble, M. Ciobanu, V. Gueguen, D. G. Castner, V. Migonney, *Biomacromolecules* **2007**, *8*, 3317.
[30] D. Missirlis, T. Haraszti, H. Kessler, J. P. Spatz, *Sci. Rep.* **2017**, *7*, 1.
[31] C. C. Liang, A. Y. Park, J. L. Guan, *Nat. Protoc.* **2007**, *2*, 329.
[32] P. Bainbridge, *J. Wound Care* **2013**, *22*, 407.
[33] A. J. Singer, R. A. F. Clark, *N. Engl. J. Med.* **1999**, *341*, 738.
[34] R. A. F. Clark, *J. Am. Acad. Dermatol.* **1985**, *13*, 701.
[35] H. Khorasani, Z. Zheng, C. Nguyen, J. Zara, X. Zhang, J. Wang, K. Ting, C. Soo, *Am. J. Pathol.* **2011**, *178*, 621.
[36] G. F. Caetano, M. Fronza, M. N. Leite, A. Gomes, M. A. C. Frade, *Pharm. Biol.* **2016**, *54*, 2555.
[37] X. Zhang, R. Xu, X. Hu, G. Luo, J. Wu, W. He, *Burns Trauma* **2015**, *3*, 15.
[38] M. A. Nosenko, S. G. Ambaryan, M. S. Drutskaya, *Mol. Biol.* **2019**, *53*, 653A.
[39] K. E. Johnson, T. A. Wilgus, *Adv. Wound Care* **2014**, *3*, 647.
[40] J. N. Israelachvili, *Intermolecular and Surface Forces*, Elsevier, Waltham, USA, **2011**. p. 482.
[41] M. L. Smith, D. Gourdon, W. C. Little, K. E. Kubow, R. A. Eguiluz, S. [illegible] lorris, V. Vogel, *PLoS Biol.* **2007**, *5*, 2243.
[42] [illegible] rosby, P. M. Schlievert, J. A. Merriman, J. M. King, W. Salgado-Pabón, A. R. Horswill, *PLoS Pathog.* **2016**, *12*, e1005604.
[43] T. Takahashi, *Methods Mol. Biol.* **2016**, 257.
[44] K. A. Lee, S. S. Lee, S. Y. Kim, A. R. Choi, J. H. Lee, K. H. Jung, *Biochim. Biophys. Acta, Gen. Subj.* **2015**, *1850*, 1694.
[45] S. L. Rennard, R. Berg, G. R. Martin, J. M. Foidart, P. G. Robey, *Anal.* [illegible] *n.* 1980, *104*, 205.
[46] [illegible] arks, N. A. Vava [illegible] L. Kasting, B. Long, M. L. Tanaka, P. A. Sanger, K. Schnell, T. A [illegible] er-Kerr, *Adv. Ski. Wound Care* **2015**, *28*, 59.
[47] R. F. Friesen, M. Wiertlewski, M. A. Peshkin, J. E. Colgate, *IEEE World Haptics Conf. (WHC)*, IEEE, Piscataway, NY **2015**, p. 208.

# An Accelerated Wound-Healing Surgical Suture Engineered with an Extracellular Matrix

Setiawati, Agustina; Jang, Dongyoon; Cho, Daeyon; Cho, Shingyu; Jeong, Hayan; Park, Sungmin; Gwak, Jungsug; Ryu, Soo Ryeon; Jung, Won Hee; Ju, Bong Gun; Jung, Kwang Hwan; Kwon, Oh Sun; Shin, Kwanwoo

01 Agustina Setiawati Page 1
11/6/2022 11:46

02 Agustina Setiawati Page 1
11/6/2022 11:46

03 Agustina Setiawati Page 1
11/6/2022 11:47

04 Agustina Setiawati Page 8
19/9/2021 15:42

05 Agustina Setiawati Page 10
28/5/2022 14:34

06 Agustina Setiawati Page 10
28/5/2022 14:34

07 Agustina Setiawati Page 10
28/5/2022 14:33

08 Agustina Setiawati Page 10
28/5/2022 14:33

# An Accelerated Wound-Healing Surgical Suture Engineered with an Extracellular Matrix

ORIGINALITY REPORT

| 20% | 15% | 18% | 5% |
|---|---|---|---|
| SIMILARITY INDEX | INTERNET SOURCES | PUBLICATIONS | STUDENT PAPERS |

PRIMARY SOURCES

| | | |
|---|---|---|
| 1 | Agustina Setiawati, Sungwoo Jeong, Albertus Ivan Brilian, Sang Ho Lee, Jin‐Gon Shim, Kwang‐Hwan Jung, Kwanwoo Shin. "Fabrication of a Tailored, Hybrid Extracellular Matrix Composite", Macromolecular Bioscience, 2022<br>Publication | 3% |
| 2 | www.pubfacts.com<br>Internet Source | 2% |
| 3 | Submitted to Xiamen University<br>Student Paper | 2% |
| 4 | www.mdpi.com<br>Internet Source | 1% |
| 5 | diseasebiophysics.seas.harvard.edu<br>Internet Source | 1% |
| 6 | microbiomejournal.biomedcentral.com<br>Internet Source | 1% |
| 7 | docksci.com<br>Internet Source | 1% |

| | | |
|---|---|---|
| 8 | www.coursehero.com<br>Internet Source | 1 % |
| 9 | Huanling Wu, Gareth R. Williams, Junzi Wu, Jianrong Wu, Shiwei Niu, Heyu Li, Haijun Wang, Limin Zhu. "Regenerated chitin fibers reinforced with bacterial cellulose nanocrystals as suture biomaterials", Carbohydrate Polymers, 2018<br>Publication | 1 % |
| 10 | Agustina Setiawati, Sungwoo Jeong, Albertus Ivan Brillian, Sang Ho Lee, Jin‐Gon Shim, Kwang‐Hwan Jung, Kwanwoo Shin. "Fabrication of a Tailored, Hybrid Extracellular Matrix Composite", Macromolecular Bioscience, 2022<br>Publication | 1 % |
| 11 | www.frontiersin.org<br>Internet Source | 1 % |
| 12 | downloads.hindawi.com<br>Internet Source | <1 % |
| 13 | pubs.rsc.org<br>Internet Source | <1 % |
| 14 | Monica Cahyaning Ratri, Albertus Ivan Brilian, Agustina Setiawati, Huong Thanh Nguyen, Veasna Soum, Kwanwoo Shin. "Recent Advances in Regenerative Tissue Fabrication: Tools, Materials, and Microenvironment in | <1 % |

Hierarchical Aspects", Advanced NanoBiomed Research, 2021
Publication

| | | |
|---|---|---|
| 15 | onlinelibrary.wiley.com<br>Internet Source | <1 % |
| 16 | www.nature.com<br>Internet Source | <1 % |
| 17 | www.researchsquare.com<br>Internet Source | <1 % |
| 18 | Yoshihito Sakurai, Norimichi Kawashima, Yoshikazu Tokuoka. "Chemical properties and protein adsorptions on ozone/UV-treated poly(ethylene terephthalate) film surfaces", Colloid and Polymer Science, 2017<br>Publication | <1 % |
| 19 | Yatma Gueye. "Trafficking and secretion of matrix metalloproteinase-2 in olfactory ensheathing glial cells: A role in cell migration?", Glia, 05/2011<br>Publication | <1 % |
| 20 | core.ac.uk<br>Internet Source | <1 % |
| 21 | Srividya Ganapathy, Odette Bécheau, Hanka Venselaar, Siebren Frölich et al. "Modulation of spectral properties and pump activity of proteorhodopsins by retinal analogues", Biochemical Journal, 2015 | <1 % |

| | | |
|---|---|---|
| | Publication | |
| 22 | repositorio.uchile.cl<br>Internet Source | <1 % |
| 23 | www.kitasato-u.ac.jp<br>Internet Source | <1 % |
| 24 | Shu-Chuan Chen, King-Song Jeng, Michael M. C. Lai. "Zinc Finger-Containing Cellular Transcription Corepressor ZBTB25 Promotes Influenza Virus RNA Transcription and Is a Target for Zinc Ejector Drugs", Journal of Virology, 2017<br>Publication | <1 % |
| 25 | digitalcommons.usu.edu<br>Internet Source | <1 % |
| 26 | journals.plos.org<br>Internet Source | <1 % |
| 27 | www.daigangbio.cn<br>Internet Source | <1 % |
| 28 | 2010.igem.org<br>Internet Source | <1 % |
| 29 | Nopparuj Soomherun, Narumol Kreua-ongarjnukool, Saowapa Thumsing Niyomthai, Sorayouth Chumnanvej. "Kinetics of Drug Release via Nicardipine Hydrochloride - loaded Carboxymethyl Cellulose/Poly(D,L - lactic - co - glycolic acid) Nanocarriers Using a | <1 % |

Contemporary Emulsion Process", ChemNanoMat, 2020
Publication

| | | |
|---|---|---|
| 30 | Tuan-Wei Sun, Ying-Jie Zhu, Feng Chen. "Highly Flexible Multifunctional Biopaper Comprising Chitosan Reinforced by Ultralong Hydroxyapatite Nanowires", Chemistry - A European Journal, 2017<br>Publication | <1 % |
| 31 | biosignaling.biomedcentral.com<br>Internet Source | <1 % |
| 32 | bora.uib.no<br>Internet Source | <1 % |
| 33 | mbio.asm.org<br>Internet Source | <1 % |
| 34 | pbiid2013.sciencesconf.org<br>Internet Source | <1 % |
| 35 | stemcellres.biomedcentral.com<br>Internet Source | <1 % |
| 36 | www.ncbi.nlm.nih.gov<br>Internet Source | <1 % |
| 37 | Jiranuwat Sapudom, Stefan Rubner, Steve Martin, Stephan Thoenes, Ulf Anderegg, Tilo Pompe. "The interplay of fibronectin functionalization and TGF-β1 presence on fibroblast proliferation, differentiation and | <1 % |

migration in 3D matrices", Biomaterials Science, 2015
Publication

| | | |
|---|---|---|
| 38 | Submitted to Universita degli Studi di Torino<br>Student Paper | <1% |
| 39 | dx.doi.org<br>Internet Source | <1% |
| 40 | electronicsandbooks.com<br>Internet Source | <1% |
| 41 | repository.ubn.ru.nl<br>Internet Source | <1% |
| 42 | Akio Nakane, Munenori Okamoto, Misako Asano, Masashi Kohanawa, Yu-ichiro Satoh, Tomonori Minagawa. " Protection by dexamethasone from a lethal infection with in mice ", FEMS Immunology & Medical Microbiology, 1994<br>Publication | <1% |
| 43 | Chao He, Chuan-Xiong Nie, Wei-Feng Zhao, Lang Ma, Tao Xiang, Chong Sage Cheng, Shu-Dong Sun, Chang-Sheng Zhao. "Modification of polyethersulfone membranes using terpolymers engineered and integrated antifouling and anticoagulant properties", Polymers for Advanced Technologies, 2013<br>Publication | <1% |

| | | |
|---|---|---|
| 44 | Mahdi Dargahi, Valentin Nelea, Aisha Mousa, Sasha Omanovic, Mari T. Kaartinen. "Electrochemical modulation of plasma fibronectin surface conformation enables filament formation and control of endothelial cell–surface interactions", RSC Adv., 2014<br>Publication | <1 % |
| 45 | Seungkuk Ahn, Christophe O. Chantre, Alanna R. Gannon, Johan U. Lind et al. "Soy Protein/Cellulose Nanofiber Scaffolds Mimicking Skin Extracellular Matrix for Enhanced Wound Healing", Advanced Healthcare Materials, 2018<br>Publication | <1 % |
| 46 | Xinxi Zeng, Han Zhang, Xiaoqing Xi, Bo Li, Ji Zhou. " Numerically Denoising Thermally Tunable and Thickness‐Dependent Terahertz Signals in ErFeO Based on Bézier Curves and ‐Splines ", Annalen der Physik, 2021<br>Publication | <1 % |
| 47 | liugroup.ucsd.edu<br>Internet Source | <1 % |
| 48 | repository.hanyang.ac.kr<br>Internet Source | <1 % |
| 49 | www.freepatentsonline.com<br>Internet Source | <1 % |
| | www.openstarts.units.it | |

| | | |
|---|---|---|
| 50 | Internet Source | <1% |
| 51 | Hongmei Liu, Yifan Cai, Yafei Zhang, Yandong Xie, Hui Qiu, Lei Hua, Xuejiao Liu, Yuling Li, Jun Lu, Longzhen Zhang, Rutong Yu. "Development of a Hypoxic Radiosensitizer-Prodrug Liposome Delivery DNA Repair Inhibitor Dbait Combination with Radiotherapy for Glioma Therapy", Advanced Healthcare Materials, 2017<br>Publication | <1% |
| 52 | Kara M. de la Harpe, Pierre P.D. Kondiah, Thashree Marimuthu, Yahya E. Choonara. "Advances in Carbohydrate-Based Polymers for the Design of Suture Materials: A Review", Carbohydrate Polymers, 2021<br>Publication | <1% |
| 53 | Maki Ishida-Takagishi. "The Dishevelled-associating protein Daple controls the non-canonical Wnt/Rac pathway and cell motility", Nature Communications, 05/29/2012<br>Publication | <1% |
| 54 | Nidhi Gupta, Santosh K. Rath, Jasvinder Singh, Arem Qayum, Shashank Singh, Payare L. Sangwan. "Synthesis of novel benzylidene analogues of betulinic acid as potent cytotoxic agents", European Journal of Medicinal Chemistry, 2017 | <1% |

Publication

| | | |
|---|---|---|
| 55 | Petra M. Krämer, Elisabeth Kremmer, Cristina M. Weber, Ioan M. Ciumasu, Stephan Forster, Antonius A. Kettrup. "Development of new rat monoclonal antibodies with different selectivities and sensitivities for 2,4,6-trinitrotoluene (TNT) and other nitroaromatic compounds", Analytical and Bioanalytical Chemistry, 2005<br>Publication | <1 % |
| 56 | Ramses Ayala, Chao Zhang, Darren Yang, Yongsung Hwang et al. "Engineering the cell–material interface for controlling stem cell adhesion, migration, and differentiation", Biomaterials, 2011<br>Publication | <1 % |
| 57 | ftp.idu.ac.id<br>Internet Source | <1 % |
| 58 | www.science.gov<br>Internet Source | <1 % |
| 59 | Hayan Jeong, Jee Youn Shin, Kwanghyun Lee, Su-Jin Lee et al. "Caffeoyl-Prolyl-Histidine Amide Inhibits Fyn and Alleviates Atopic Dermatitis-Like Phenotypes via Suppression of NF-κB Activation", International Journal of Molecular Sciences, 2020<br>Publication | <1 % |

60 Nipapan Ruecha, Jumi Lee, Heedo Chae, Haena Cheong et al. "Paper-Based Digital Microfluidic Chip for Multiple Electrochemical Assay Operated by a Wireless Portable Control System", Advanced Materials Technologies, 2017
Publication

<1%

| | | | |
|---|---|---|---|
| Exclude quotes | Off | Exclude matches | Off |
| Exclude bibliography | On | | |